Journal of Solid State Electrochemistry (2019) 23:1787–1794
https://doi.org/10.1007/s10008-019-04280-y

ORIGINAL PAPER

Highly efficient, PbS:Hg quantum dot–sensitized, plasmonic solar cells with TiO_2 triple-layer photoanode

M.A.K.L. Dissanayake[1,2] · T. Jaseetharan[1,2,3] · G.K.R. Senadeera[1,4] · J.M.K.W. Kumari[1] · C.A. Thotawatthage[1,2] · B-E. Mellander[5] · I. Albinson[6] · M. Furlani[5]

Received: 22 February 2019 / Revised: 13 April 2019 / Accepted: 18 April 2019 / Published online: 10 May 2019

Abstract

Highly efficient, PbS:Hg quantum dot–sensitized, plasmonic solar cells with TiO_2 triple-layer photoanode were fabricated by successive ionic layer adsorption and reaction (SILAR) method. These nanostructured photoanodes were characterized by optical and morphological techniques and the solar cells were characterized by optical and electrical techniques. The light absorption by the photoanode was enhanced by effective light scattering process using a triple-layer TiO_2 nanostructure, fabricated with a TiO_2 nanofiber layer sandwiched between two TiO_2 nanoparticle layers. The best plasmon-enhanced quantum dot–sensitized solar cell showed an efficiency of 5.41% with short circuit current density of 18.02 mA cm^{-2} and open-circuit voltage of 679.83 mV. The overall efficiency and photocurrent density of the Q-dot-sensitized solar cell are enhanced by 15.84% and 38.83% respectively due to the plasmonic effect. The enhanced efficiency appears to be due to the improved short circuit current density by increased light absorption by the triple-layered photoanode nanostructure as well as by the localized surface plasmon resonance (LSPR) effect of the plasmonic gold nanoparticles. This is the first report on plasmon-enhanced, triple-layered TiO_2 photoanode sensitized with PbS:Hg Q-dots.

Keywords Triple-layer TiO_2 photoanode · PbS:Hg quantum dots · Plasmonic effect · Solar cells

Introduction

Semiconductor colloidal quantum dots (Q-dots) are among the promising materials for the future electronic and optoelectronic devices including solar cells and detectors [1–5]. During the past decade, they have been intensively studied for numerous applications due to their excellent optoelectronic properties such as the high molar extinction coefficients, tunable energy gap, and ability of multiple exciton generation [6, 7].

Q-dot-sensitized solar cells have emerged as the cost-effective third-generation solar cells in the solar energy conversion processes and also one of the main applications of colloidal Q-dots. TiO_2, SnO_2, and ZnO semiconductor

Highlights
- Gold nanoparticle–incorporated, Hg-PbS quantum dot–sensitized photoanode was made.
- DSSCs fabricated with above photoanode showed an efficiency of 5.41%.
- Efficiency enhancement of 38.8% was achieved by a plasmonic resonance effect.

✉ M.A.K.L. Dissanayake
makldis@yahoo.com

[1] National Institute of Fundamental Studies, Hantana Road, Kandy, Sri Lanka

[2] Postgraduate Institute of Science, University of Peradeniya, Peradeniya, Sri Lanka

[3] Department of Physical Sciences, South Eastern University of Sri Lanka, Sammanthurai, Sri Lanka

[4] Department of Physics, The Open University of Sri Lanka, Nawala, Nugegoda, Sri Lanka

[5] Department of Applied Physics, Chalmers University of Technology, Gothenburg, Sweden

[6] Department of Physics, University of Gothenburg, Gothenburg, Sweden

nanoparticle-based electrodes are used as photoanodes in Q-dot-sensitized solar cells. To enhance the power conversion efficiency of Q-dot-sensitized solar cell, there are several techniques that have been reported. Improving the light harvesting by scattering using modified photoanodes, enhancing the photocurrent further by plasmonic effect, and using an efficient electrolyte and counter electrode are some of these techniques. Enhancement through the efficient light harvesting using nanostructurally modified TiO_2 photoanodes based on nanofibers, nanocorals, nanotubes, nanowires, and nanohelixes has been studied [8–12]. Recently, TiO_2 nanoparticle/nanofiber/nanoparticle triple-layered photoanode-based solar cells have been reported by us [13–15].

The efficiency of solar cells can be enhanced by using the plasmonic nanostructures. These nanostructures are capable of increased light trapping by plasmonic resonance effect. Plasmonic nanostructures can be placed at the top of, within, or at the base of photovoltaic devices. Free electrons on the metal surface can have strong interaction with the light. When the frequency of the incident photons matches with the frequency of these free electrons, it will lead to collective oscillations of the electrons and this oscillation is defined as localized surface plasmon resonance (LSPR) [16]. Plasmonic enhancement in photovoltaic devices occurs due to (i) the LSPR relaxation and re-emission of light acting as a secondary light source that develops the local electric field and (ii) the LSPR relaxation transferring the energy to the conduction band of the semiconductor thereby enhancing the photocurrent [17]. Wavelength of the LSPR depends on the size and shape of the plasmonic particles, inter-particle distance, volume fraction of the metal in the surrounding material, and the dielectric constant of the surrounding material such as TiO_2 nanostructure [18]. Plasmonic nanoparticles are highly polarizable at their resonance frequency. At this frequency, these nanoparticles show high optical absorption and high scattering cross-sections. In the case of Au and Ag nanoparticles, the resonance frequencies are in the visible region [19]. Therefore, these plasmonic nanoparticles can be used for enhanced visible light harvesting by LSPR effect.

Metallic nanoparticles such as Au, Ag, and Zn have been studied due to their exceptional optical properties in various fields including photovoltaics. In addition to the metallic nanoparticles, different shapes of metallic plasmonic materials such as nanoclusters, hemisphere, and core-shell sphere can also be used. In dye-sensitized solar cells, metallic nanoparticles have been used to enhance the light trapping [20–24]. PbS/ZnO nanowire bulk-heterojunction Q-dot-sensitized solar cell with plasmonic silver nanocubes has been reported with an overall efficiency of 6.03% [25]. More recently, TiO_2/Au nanoparticle-based CdS/CdSe core-shell Q-dot-sensitized solar cells have been fabricated with an efficiency of 6.00% [26]. In another study, Ag plasmonic nanostructure–incorporated TiO_2/CdS Q-dot-sensitized solar cell with 6.00% efficiency has been reported [27]. Tokuhisa Kawawaki et al. [28] recently reported a significant efficiency enhancement due to plasmonic gold nanoparticles in solar cells sensitized with PbS quantum dots. PbS quantum dots have gained a great attention in various studies due to their excellent optoelectronic properties. PbS has a high absorption coefficient in the order of 10^5 cm^{-1} and wide range of tunable energy gap [29]. Moreover, they have relatively large exciton Bohr radius of 18 nm that allows tuning their band gap in the range from 0.50 to 5.50 eV [30, 31]. According to the quantum confinement effect, by controlling the size of the PbS Q-dots, the absorption wavelength of the first exciton peak can easily be shifted towards the infrared region to harvest the near infrared and infrared photons for the photovoltaic applications.

In this study, Hg-doped PbS Q-dots were deposited using SILAR method on plasmonic Au nanoparticle–incorporated TiO_2 tri-layer photoanode structure and the solar cells were fabricated and characterized. Jin-Wook Lee et al. [29] using extended X-ray absorption fine structure (EXAFS) have established the nature and the presence of Hg in the photoanode. Further, it has been revealed that the Pb-S bond distance is decreased by the Hg doping leading to bond reinforcement and reduced structural disorder enhanced electron injection. The overall performance of the solar cells has been enhanced due to the plasmonic effect. To the best of our knowledge, this is the first report on plasmon-enhanced triple-layered TiO_2 electrode sensitized with PbS:Hg Q-dots.

Experimental

Materials

Fluorine-doped tin oxide (FTO) coated glass (8 Ω cm^{-2}, Solarnoix), titanium (IV) isopropoxide (97%, Fluka), propan-1-ol (99.9%, Fisher), glacial acetic acid (99%, Fisher), titanium dioxide P-90 powder (Evonik), titanium dioxide powder P-25 (Degussa), sulfur (99%, Daejng), triethanolamine (99%, Fluka), ethanol (96%, BDH) and hydrogen tetrachloroaurate (III) (99.9%), trisodium citrate dihydrate (99%), mercury (II) chloride (99.5%), sodium sulfide hydrate (> 60%), N,N-dimethyl formamide (99%), potassium chloride (99%), lead (II) nitrate (99%), poly ethylene glycol (99.8%), Triton X-100, hydrochloric acid (37%), and methanol (99.8%) all from Sigma-Aldrich were used as received.

Preparation of the Au nanoparticles

Au nanoparticle solution was synthesized using the citrate reduction method as described by Huang et al. [32]. 0.1 g of $Na_3C_6H_5O_7$ was dissolved in 10 ml of de-ionized water and 1 mM of $HAuCl_4$ solution was prepared with 20 ml de-ionized

water. This solution was boiled under continuous stirring and 2 ml of $Na_3C_6H_5O_7$ solution was added to the boiling $HAuCl_4$ solution. When the color of the mixture became deep red, the hotplate was turned off and the solution was allowed to cool.

Preparation of the TiO_2 triple-layer nanostructure

TiO_2 compact layer solution was prepared with 8 ml of ethanol, 1 ml of propan-1-ol, 1 ml of glacial acetic acid, 1 ml of titanium (IV) isopropoxide, and 1 drop of conc. HNO_3. This solution was used to spin coat the first TiO_2 compact layer on pre-cleaned FTO glass substrate at 3000 rpm for 1 min and the layer was sintered at 120 °C for 5 min. Again, the same spin coating process was repeated to form the second TiO_2 compact layer on the first compact layer and both layers were subsequently sintered at 450 °C for 45 min. A paste was prepared by grinding 0.25 g of TiO_2 P-90 powder with 1 ml of 0.1 M HNO_3 and it was spin-coated on the TiO_2 compact bilayer structure at 3000 rpm for 1 min and the resulting photoanode was subsequently sintered at 450 °C for 45 min. 0.25 g of TiO_2 P-25 powder was added to 10 drops of 0.1 M HNO_3 and one drop of triton X-100 and the mixture was ground for 15 min. Then, 0.05 g of polyethylene glycol was added to the mixture and appropriate amount of 0.1 M HNO_3 was added to the mixture and creamy paste was obtained. In order to study the plasmonic effect, different concentrations of Au nanoparticle colloidal were added and the paste was ground further 15 min to get a homogeneous distribution of Au nanoparticles in the TiO_2 P-25 paste. The TiO_2 P-25 nanoparticle paste containing Au nanoparticles was spin-coated on TiO_2 P-90 layer at 1000 rpm for 1 min for each Au nanoparticle concentration. Finally, the electrodes were sintered for 45 min at 450 °C. The Q-dot-sensitized solar cells fabricated with FTO/compact layer/TiO_2 P-90/TiO_2 P-25 photoanode incorporating 0.45 ml of Au NP colloidal solution were found to exhibit the highest solar cell efficiency.

TiO_2 nanofiber layer was prepared by the following method described by us in an earlier report [13]. Initially, 9.5 ml of N, N-dimethyl formamide and 0.5 ml of glacial acetic acid were thoroughly mixed. Subsequently, 1.5 ml of titanium (IV) isopropoxide was added to the mixture which was subjected to magnetic stirring for 20 min. Finally, 0.75 g of poly (vinylacetate) was added to the mixture and magnetically stirred for 4 h. A TiO_2 nanofiber layer was deposited for 20 min with a solution flow rate of 2 ml h^{-1} on the Au nanoparticle–incorporated TiO_2 P-25 layer by electrospinning (NaBond Electrospinner, NaBond Technologies, Hong Kong). During the electrospinning, the voltage difference and the distance between the spinneret and photoanode were kept at 15 kV and 6.5 cm respectively. The electrodes FTO/TiO_2 compact layer/TiO_2 P-90/TiO_2 P-25 covered with Au nanoparticles/TiO_2 layer were sintered at 450 °C for 45 min. In order to fabricate the tri-layer photoanode, another Au-incorporated TiO_2 P-25 layer was deposited on the TiO_2 nanofiber layer using a spin coater with rpm of 1000 for 1 min. Finally, the electrodes were sintered 450 °C for 45 min.

Preparation of PbS:Hg Q-dot-sensitized TiO_2 photoanodes

PbS:Hg quantum dots were incorporated to each layer of TiO_2 triple-layer photoanode by SILAR method [13]. For the preparation of cationic precursor solution, 0.1 M $Pb(NO_3)_2$, 0.8 M triethanolamine, and 6 mM $HgCl_2$ were dissolved in de-ionized water. 0.1 M Na_2S was dissolved in de-ionized water for anionic precursor solution. Based on previous trails, 6 SILAR cycles were found to give the highest efficiency solar cells and therefore 6 SILAR cycles were used to deposit PbS:Hg Q-dots on each TiO_2 layer in the composite photoanode structure [13]. In each SILAR cycle, TiO_2 electrode was dipped for 1 min in the cationic precursor and for 1.5 min in the anionic precursor solution. Between each dipping process, the composite photoanode was washed with de-ionized water. Finally, PbS:Hg Q-dot-sensitized photoanode was sintered at 120 °C for 10 min and immersed in a solution of 0.1 M Na_2S for 1 min at room temperature. Then, the photoanode was washed with de-ionized water and dried. A Q-dot-sensitized solar cell with an identical TiO_2 triple-layer photoanode nanostructure (nanoparticle/nanofiber/nanoparticle) sensitized with PbS:Hg Q-dots, but without colloidal Au nanoparticles, was also fabricated and used as the control device.

Optical absorption measurements

Optical absorption spectra of Au nanoparticle colloidal, TiO_2 triple-layer, TiO_2 triple-layer with Au nanoparticles, and PbS:Hg quantum dots were taken using a Shimadzu 2450 spectrophotometer in the 350–1100-nm wavelength range.

Preparation of the polysulfide electrolyte

Polysulfide electrolyte was prepared as described previously [13]. 2 M Na_2S, 2 M S, and 0.2 M KCl were dissolved in a 7:3 (*v*/*v*) mixture of methanol and water. The mixture was magnetically stirred at room temperature until the solution became clear deep-orange color.

Preparation of the counter electrode

A brass plate of size 2 cm × 1 cm was cleaned with concentrated HCl at 80 °C. A mask with 0.12 cm^2 hole was fixed on the cleaned brass plate and the unmasked area was covered with the polysulfide electrolyte. The Cu_2S layer formed on this brass plate was used as a counter electrode.

Current–voltage characterization

Current–voltage characterization of each type of PbS:Hg Q-dot-sensitized solar cells with an active area of 0.12 cm^2 was measured under illumination of 100 mW cm^{-2} with AM 1.5 filter using a computer-controlled setup consisting of a multimeter (Keithley 2000) connected to a potentiostat/galvanostat unit (HA-301).

Electrochemical impedance measurements

Electrochemical impedance spectroscopy (EIS) provides an important tool to study the interfaces between electrodes and electrolytes. EIS spectra of all Q-dot-sensitized solar cells were collected by Autolab potentiostat/galvanostat PGSTAT128 N with frequency response analyzer (Metrohm) in a frequency range between 0.01 Hz and 1 MHz under the simulated light of 100 mW cm^{-2} with AM 1.5 filter. Important electrochemical parameters such as charge transfer resistance, series resistance, recombination resistance, and electron lifetime were estimated using the fitted equivalent circuit.

Results and discussion

Morphology of the TiO_2 triple-layer photoanode

The cross-section SEM image of the TiO_2 triple-layer (nanoparticle/nanofiber/nanoparticle) composite structure is shown in Fig. 1. Total thickness of the TiO_2 triple-layer is around 3.4 μm. The detailed configuration of the composite photoanode can be represented as follows: glass substrate with FTO layer/TiO_2 compact layer/TiO_2 P-90 nanoparticle layer (0.6 μm)/TiO_2 P-25 nanoparticle layer (1.3 μm)/TiO_2 nanofiber layer (0.8 μm)/TiO_2 P-25 nanoparticle layer (1.3 μm).

Optical absorption of Au nanoparticles and photoanodes

Figure 2 depicts the optical absorption spectrum of synthesized plasmonic colloidal Au nanoparticles showing a broad absorption in the visible region which peaks around 527 nm. From this absorption maximum, the average particle size of the Au nanoparticles has been estimated, which is in the range of 25–35 nm and the shape of the particles is spherical [33]. Stephan Link et al. [34] reported that, Au nanoparticles which have the diameter greater than 25 nm, the plasmon bandwidth increases with increasing size as the wavelength of the interacting light becomes comparable with the dimension of the nanoparticle. And also, the extinction coefficient depends on the size of the nanoparticle.

Figure 3 displays the optical absorption spectra of the TiO_2 triple-layer and Au nanoparticle–incorporated TiO_2 triple-layer with and without sensitization by PbS:Hg quantum dots. Bare TiO_2 nanoparticle/nanofiber/nanoparticle nanostructure also shows increased optical absorption in the visible region (Fig. 3, curve (b)), quite likely due to the multiple light scattering events within the triple-layer. Au nanoparticle–incorporated TiO_2 triple-layer photoanode shows a broad peak in the visible region between 500 and 550 nm (Fig. 3, curve (c)). This peak clearly confirms the presence of Au plasmonic nanoparticles in the TiO_2 triple-layer nanostructure as described by Yin-Cheng Yen et al. [2]. The plasmonic absorption peak due to synthesized colloidal Au nanoparticles appears around 527 nm (Fig. 2). Correspondingly, the PbS:Hg Q-dot-sensitized, Au nanoparticle–incorporated TiO_2 triple-layer photoanode shows a broad peak around 500–550 nm

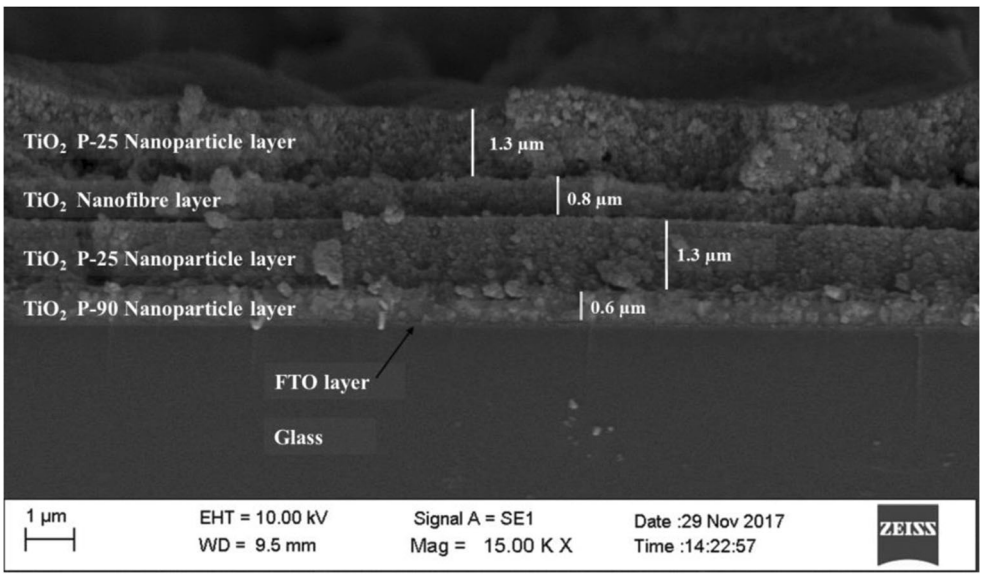

Fig. 1 SEM image of cross-section of the TiO_2 triple-layer photoanode. From the bottom: glass substrate with FTO layer/TiO_2 compact layer/TiO_2 P-90 nanoparticle layer (0.6 μm)/TiO_2 P-25 nanoparticle layer (1.3 μm)/TiO_2 nanofiber layer (0.8 μm)/TiO_2 P-25 nanoparticle layer (1.3 μm)

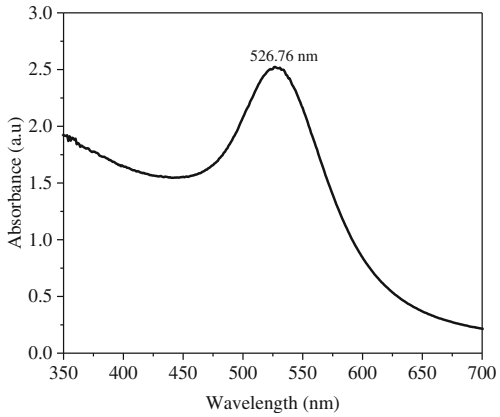

Fig. 2 Optical absorption spectrum of colloidal Au nanoparticles

superimposed on an enhanced overall absorption curve (Fig. 3(d)). The cumulative effect due to the presence of TiO_2 nanofibers (scattering enhanced), Au nanoparticles (plasmonic enhanced), and PbS:Hg Q-dots sensitized in the sandwich structure has resulted an overall increase in the optical absorption significantly. Also, this photoanode exhibits another very strong absorption peak at around 1050 nm in the near IR region evidently due to the optical absorption by PbS:Hg Q-dots [35]. The size of the PbS:Hg quantum dots corresponding to the absorption of 1050 nm can been estimated to be in the range of 3–4 nm [31, 35].

Figure 4 depicts the plots of $(Ah\nu)^2$ against $(h\nu)$ for the TiO_2 triple-layer structure with and without Au plasmonic nanoparticles. Here, A is the absorption coefficient and ν is the frequency. According to these plots, the estimated value of the optical energy band gap for the TiO_2 triple-layer electrode is 3.42 eV and for the Au nanoparticle–incorporated TiO_2 triple-layer electrode is 3.04 eV. This result clearly shows that the energy band gap of the TiO_2 semiconductor nanostructure has reduced by the defect-induced band gap narrowing caused

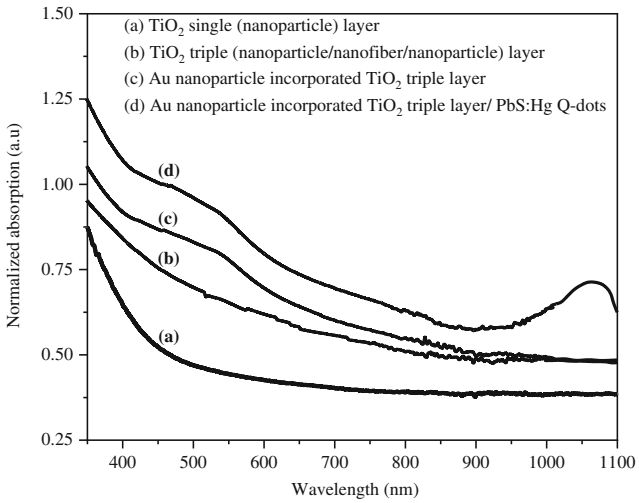

Fig. 3 Normalized absorption spectra of (a) TiO_2 single layer; (b) TiO_2 triple-layer; (c) Au nanoparticle–incorporated TiO_2 triple-layer; (d) Au nanoparticle–incorporated TiO_2 triple-layer with PbS:Hg quantum dots

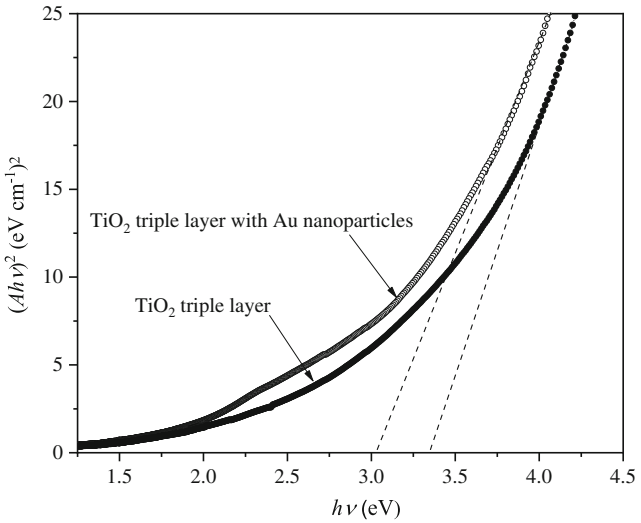

Fig. 4 Plots of $(Ah\nu)^2$ versus $(h\nu)$ for the TiO_2 triple-layer photoanode structures with and without Au plasmonic nanoparticles

by the presence of Au plasmonic nanoparticles. Similar observations have been made by other groups too [22, 36, 37].

Photovoltaic characteristics of the solar cells

Current density (J) vs voltage (V) measurements have been performed to obtain the photovoltaic parameters of solar cells. Figure 5 displays the J-V plots for the PbS:Hg Q-dot-sensitized solar cells with TiO_2 triple-layer photoanodes with and without Au nanoparticles under the simulated sunlight of 100 mW cm^{-2} with AM 1.5 spectral filter. Au nanoparticle–incorporated PbS:Hg Q-dot-sensitized solar cells show improved photovoltaic performance compared with the controlled device. The results are summarized in Table 1.

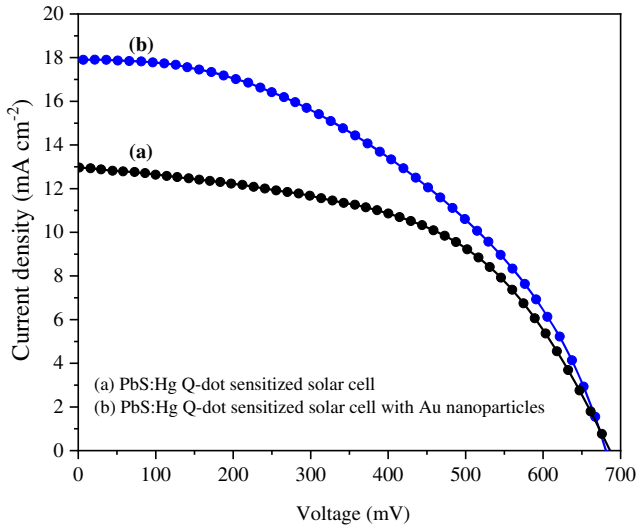

Fig. 5 Current density–voltage curves of PbS:Hg Q-dot-sensitized solar cell–based TiO_2 triple-layer photoanode (a) without Au nanoparticles and (b) with Au nanoparticles

Table 1 Photovoltaic parameters of PbS:Hg Q-dot-sensitized solar cells fabricated with (a) TiO_2 triple-layer (b) Au nanoparticle–incorporated TiO_2 triple-layer

TiO_2 photoanode	J_{SC} (mA cm^{-2})	V_{OC} (mV)	*FF* (%)	Efficiency (%)
(a) Without Au NPs	12.98	686.11	52.42	4.67
(b) With Au NPs	18.02	679.83	44.21	5.41

The overall efficiency of the cell is enhanced by 15.84% due to the Au plasmonic nanoparticles. As seen from Fig. 5, this is evidently due to the enhanced photocurrent in the Q-dot-sensitized solar cell with Au nanoparticles, compared with device without Au nanoparticles, under similar fabrication and light conditions caused by the localized surface plasmon resonance (LSPR) effect [19, 38]. Au nanoparticle–incorporated Q-dot-sensitized solar cell gives a significantly higher photocurrent density of 18.02 mA cm^{-2} while the controlled device shows a lower value of 12.98 mA cm^{-2}. Clearly, the photocurrent density is enhanced by about 38.83% by the plasmonic effect due to Au nanoparticles.

Table 2 shows the variation of efficiency of the Q-dot-sensitized solar cell with the amount of colloidal Au nanoparticles. Optimum amount of colloidal Au nanoparticles added to the TiO_2 P-25 nanoparticle paste is around 0.45 ml which gives a highest overall efficiency of 5.41% corresponding to the amount of 0.45 ml added to the TiO_2 P-25 nanoparticle colloidal paste then decreases.

Electrochemical impedance spectra

In order to estimate and compare the charge transfer resistance, series resistance, and recombination resistance of the Q-dot-sensitized solar cells, electrochemical impedance spectra of the Au plasmonic Q-dot-sensitized solar cell and the controlled

Table 2 Variation of efficiency with the amount of colloidal gold nanoparticles added to the TiO_2 P-25 paste

Amount of Au nanoparticles added to the TiO_2 P-25 paste (ml)	Efficiency (%)
0.00	4.67
0.10	4.81
0.20	4.94
0.30	5.10
0.35	5.26
0.40	5.32
0.45	5.41
0.50	5.33
0.55	5.18
0.60	5.02

Table 3 EIS parameters of PbS:Hg Q-dot-sensitized solar cell with and without Au plasmonic nanoparticles

TiO_2 photoanode	R_S (Ω)	R_{1CT} (Ω)	R_{2CT} (Ω)	Z_w (Ω)
(a) Without Au nanoparticles	20.6	104.1	122.6	11.26
(b) With Au nanoparticles	39.2	156.2	188.2	9.92

Q-dot-sensitized solar cell were analyzed using the most fitting equivalent circuit for the Q-dot-sensitized solar cell. Figure 6 exhibits the corresponding Nyquist plots and the equivalent circuit used for the analysis. In this equivalent circuit, R_s is the series resistance of the FTO/TiO_2 interface and R_{1CT} represents the resistance of the counter electrode/electrolyte interface. R_{2CT} represents the resistance of the photoanode/electrolyte interface which is generally known as the "recombination resistance." CPE_1 and CPE_2 represent the constant phase elements related to the interfaces. Z_w refers to the finite Warburg impedance which originates from the difference of the diffusion coefficients of the positive and negative ions, and from the non-blocking character of the electrodes [39]. Figure 6 clearly shows that the series resistance of the Q-dot-sensitized solar cell is reduced due to the plasmonic effect.

Estimated electrochemical impedance parameters of the interfaces are given in Table 3. Au plasmonic nanoparticle–incorporated PbS:Hg Q-dot-sensitized solar cell shows low series and charge transfer resistances than the controlled Q-dot-sensitized solar cell. It is clear that the electron injection to the conduction band of the TiO_2 and the charge transfer has been enhanced by the plasmonic Au nanoparticles. Plasmonic enhanced Q-dot-sensitized solar cell shows a high recombination resistance of 188.2 Ω compared with the controlled cell. Due to the increase in the recombination resistance, it is

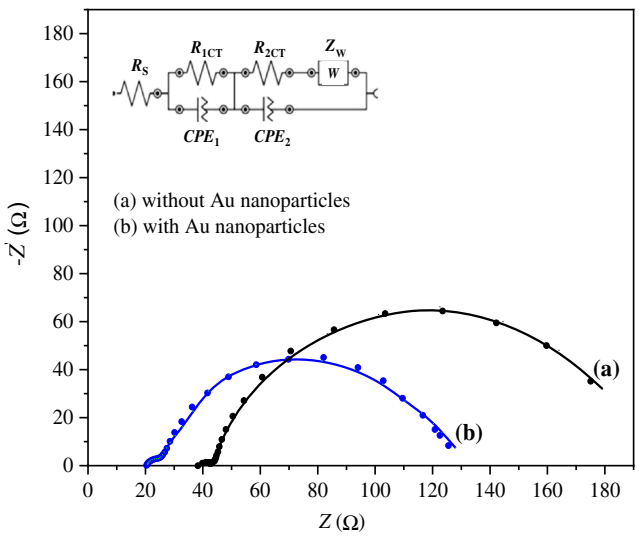

Fig. 6 Nyquist plots of the PbS:Hg Q-Dot-sensitized solar cells made with TiO_2 triple-layer photoanode structures (a) without Au nanoparticles and (b) with Au nanoparticles (solid lines represent the simulated data)

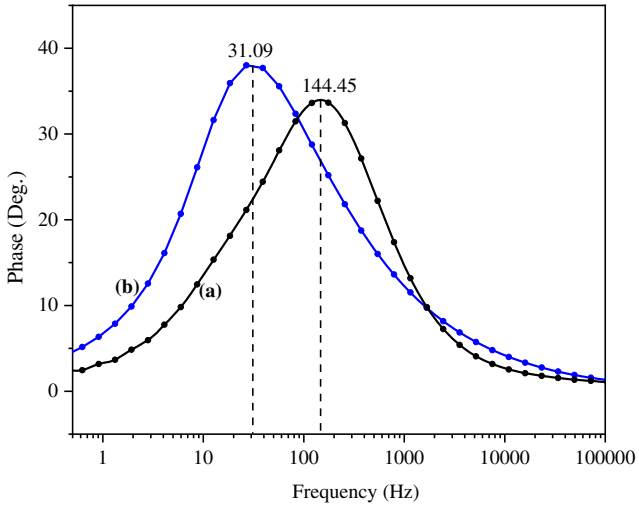

Fig. 7 Bode plots of PbS:Hg Q-dot-sensitized solar cells (a) without Au nanoparticles and (b) with Au nanoparticles

difficult for the photogenerated electrons to recombine with holes in the electrolyte. This results in the decrease of charge recombination and enhances the photocurrent [40].

Warburg impedance Z_w gives the characteristics of the diffusing species. In this study, S^{2-} and S_n^{2-} are the species in redox couple. Z_w values of Au plasmonic nanoparticle–incorporated PbS:Hg Q-dot-sensitized solar cell and controlled Q-dot-sensitized solar cell are 9.92 Ω and 11.26 Ω respectively. Au plasmonic nanoparticle–incorporated PbS:Hg Q-dot-sensitized solar cell shows a lower value of Z_w; this shows the better diffusion of electrolyte. Due to the better electrolyte diffusion, electron transport is enhanced and the performance of the Q-dot-sensitized solar cell is enhanced as described in Hee-Je Kim et al. [41].

Figure 7 shows the Bode plate of the PbS:Hg Q-dot-sensitized solar cell. The frequency peak of the Au nanoparticle–incorporated Q-dot-sensitized solar cell shifted to lower frequency. Lifetime of the electrons in the TiO_2 nanostructure can be calculated from Eq. (1). The electron lifetime is directly proportional to the recombination resistance [40].

$$\tau = \frac{1}{2\pi f_{\max}} \tag{1}$$

where f_{max} is the maximum frequency of the middle frequency peak in the Bode plot

Table 4 Comparison of electron lifetime and photovoltaic parameters of PbS:Hg Q-dot-sensitized solar cells with and without Au nanoparticles

Photoanode	f_{max} (Hz)	τ (ms)	J_{SC} (mA cm^{-2})	Efficiency (%)
(a) Without Au nanoparticles	144.45	1.10	12.98	4.67
(b) With Au nanoparticles	31.09	5.12	18.02	5.41

Table 4 shows the comparison of calculated electron lifetime and short circuit current density of each Q-dot-sensitized solar cell. Plasmon-enhanced PbS:Hg Q-dot-sensitized solar cell shows a high electron lifetime of 5.12 ms than the controlled cell. Lifetime of the electron is enhanced by 4.6 times. Therefore, electrons have a longer lifetime and are effectively transferred, substantially enhancing the photocurrent and the efficiency as discussed by Dinah Punnoose et al. [42], Yen et al. [43] and Jianjun Tian et al. [40].

Conclusion

PbS:Hg colloidal quantum dot–sensitized solar cells have been fabricated using TiO_2 triple-layer photoanode nanostructure, nanoparticle/nanofiber/nanoparticle layers. Au plasmonic nanoparticles have been incorporated into the two nanoparticle layers. These Q-dot-sensitized, plasmonic solar cells show a significantly higher efficiency of 5.41% compared with the control device without Au nanoparticles. The enhancement is evidently due to the increased short circuit photocurrent by localized surface plasmon resonance effect and defect-induced energy band gap narrowing of TiO_2 by Au nanoparticles.

Acknowledgments The authors would like to thank the Department of Physics at University of Jaffna, Sri Lanka, for providing facilities for optical absorption measurements.

Funding information This research was financially supported by the South Eastern University of Sri Lanka and Postgraduate Research Scholarship Award (NSF/SCH/2018/4) by the National Science Foundation, Sri Lanka.

References

1. Yuan M, Liu M, Sargent EH (2016) Colloidal quantum dot solids for solution-processed solar cellsColloidal quantum dot solids for solution-processed solar cells. J Nature Energy 1:16016
2. Carey GH, Abdelhady AL, Ning Z, Thon SM, Baker OM, Sargent EH (2015) Colloidal quantum dot solar cells. J Chem Rev 11: 12732–12763
3. Kim MR, Ma D (2015) Quantum-dot-based solar cells: recent advances, strategies, and challenges. J Phys Chem Lett 6:85–99
4. Mc Donald SA, Konstantatos G, Zhang S, Cyr PW, Klem EJD, Levina L, Sargent EH (2005) Solution-processed PbS quantum dot infrared photodetectors and photovoltaics. Nature materials 4: 138–142
5. Sargent EH (2008) Solution-processed infrared optoelectronics: photovoltaics, sensors, and sources. IEEE J Sel Top Quantum Electron 14:1223–1229
6. Tian J, Cao G (2013) Semiconductor quantum dot-sensitized solar cells. Nano Reviews 4:22578–22586
7. Chen G, Seo J, Yang C, Prasad PN (2013) Nanochemistry and nanomaterials for photovoltaics. J Chem Soc Rev 42:8304–8338

8. Li Y, Wei L, Chen X, Zhang R, Sui X, Chen Y, Jiao J, Mei L (2013) Efficient PbS/CdS co-sensitized solar cells based, on TiO_2 nanorod arrays. Nanoscale Res Lett 8:67–74
9. Mali SS, Desai SK, Kalagi SS, Betty CA, Bhosale PN, Devan RS, Ma YR, Patil PS (2012) PbS quantum dot sensitized anatase TiO_2 nanocorals for quantum dot-sensitized solar cell applications. Dalton Trans 41:6130–6136
10. Xu F, Benavides J, Ma X, Cloutier SG (2012) Interconnected TiO_2 nanowire networks for PbS quantum dot solar cell applications. J Nanotechnology 9:709031–709037
11. Ratanatawanate C, Xiong C, Balkus KJ (2008) Fabrication of PbS quantum dot doped TiO_2 nanotubes. ACS Nano 2:1682–1688
12. Lee SH, Jin H, Kim DY, Song K, Oh SH, Kim S, Schubert EF, Kim JK (2014) Enhanced power conversion efficiency of quantum dot sensitized solar cells with near single-crystalline TiO_2 nanohelixes used as photoanodes. Optical Express 22:867–879
13. Dissanayake MAKL, Jaseetharan T, Seenadeera GKR, Thotawatthage AC (2018) A novel, PbS:Hg quantum dot-sensitized, highly efficient solar cell structure with triple layered TiO_2 photoanode. J Electrochimica Acta 269:172–179
14. Dissanayake MAKL, Sarangika HNM, Seenadeera GKR, Divarathna HKDWMNR, Ekanayake EMPC (2017) Application of a nanostructured, tri-layer TiO_2 photoanode for efficiency enhancement in quasi-solid electrolyte-based dye- sensitized solar cells. J Appl Electrochem 47:1239–1249
15. Dissanayake MAKL, Divarathna HKDWMNR, Dissanayake CB, Seenadeera GKR, Ekanayake PMPC, Thotawattage CA (2016) An innovative TiO_2 nanoparticle/ nanofibre/ nanoparticle, three layer, composite photoanode for efficiency enhancement in dye-sensitized solar cells. J Photochem and Photobio A: Chemistry 323: 110–118
16. Ye W, Long R, Huang H, Xiong Y (2017) Plasmonic nanostructures in solar energy conversion. J Mater Chem 5:1008–1021
17. Erwin WR, Zarick HF, Talbert EM, Bardhan R (2016) Light trapping in mesoporous solar cells with plasmonic nanostructures. J Energy Env Sci 9:1577–1601
18. Mathpal MC, Kumar P, Tripathi AK, Balasubramaniyan R, Kumar Singh M, Chung JS, Agarwal A (2015) Facile deposition and plasmonic resonance of Ag–Au nanoparticles in titania thin film. New J Chem 39:6522–6530
19. Smith JG, Faucheaux JA, Jain PK (2015) Plasmon resonances for solar energy harvesting: A mechanistic outlook. Nano Today 10: 67–80
20. Luan X, Wang Y (2014) Plasmon-enhanced performance of dye-sensitized solar cells based on electrodeposited Ag nanoparticles. J Mater Sci Tech 30:1–7
21. Standridge SD, Schatz GC, Hupp JT (2009) Distance dependence of plasmon - enhanced photocurrent in dye-sensitized, solar cells. J Am Chem Soc 131:8407–8409
22. Dissanayake MAKL, Kumari JMKW, Senadeera GKR, Thotawatthage CA (2016) Efficiency enhancement in plasmonic dye-sensitized solar cells, with TiO_2 photoanodes incorporating gold and silver, nanoparticles. J Appl Electrochem 46:47–58
23. Muduli S, Game O, Dhas V, Vijayamohanan K, Bogle KA, Valanoor N, Ogale SB (2012) TiO_2–Au plasmonic nanocomposite for enhanced dye-sensitized solar cell (DSSC) performance. J Solar Energy 86:1428–1434
24. Chou CH, Yang RY, Yeh CK, Lin YJ (2009) Preparation of TiO_2/ nano-metal composite particles and their applications in dye-sensitized solar cells. J Powder Technology 194:95–105
25. Kawawaki T, Wang H, Kubo T, Saito K, Nakazaki J, Segawa H, Tatsuma T (2015) Efficiency enhancement of PbS, quantum dot/ ZnO nanowire bulk-heterojunction solar cells by plasmonic silver nanocubes. ACS Nano 9:4165–1472
26. Wang Y, Zhang Q, Huang F, Li Z, Zheng YZ, Tao X, Cao G (2018) In situ assembly of well-defined Au nanoparticles in TiO_2 films for Plasmon - enhanced quantum dot sensitized solar cells. J Nano energy 44:135–143
27. Naresh Kumar P, Deepa M, Srivastava AK (2015) Ag plasmonic nanostructures and a novel gel electrolyte in a high efficiency TiO_2/ CdS solar cell. J Phy Chem Chem Phy 17:10040–10052
28. Kawawaki T, Tatsuma T (2013) Enhancement of PbS quantum dot-sensitized photocurrents using plasmonic gold nanoparticles. J Phy Chem Chem Phy 15:20247–20251
29. Lee JW, Son DY, Ahn AK, Shi HW, Kim IY, Hwang SJ, Ko MJ, Su S, Han H, Park NG (2013) Quantum dot-sensitized solar cell with unprecedentedly high photocurrent. Sci Rep 3:1050
30. Azpiroz JM, Ugalde JM, Etgar L, Infante I, De Angelis F (2013) The Effect of TiO_2 morphology on the electron injection efficiency in PbS quantum dot solar cells: a first-principles study. J Phy Chem Chem Phy 17:6076–6086
31. Tang J, Sargent EH (2011) Infrared colloidal quantum dots for photovoltaics: Fundamentals and recent progress. J Adv Mater 23:12–29
32. Huang H, Yang X (2003) Chitosan mediated assembly of gold nanoparticles multilayer. Colloids and Surfaces A Physicochem Eng Aspects 226:77–86
33. Link S, El-Sayed MA (1999) Size and temperature dependence of the plasmon absorption of colloidal gold nanoparticles. J Phy Chem B 103:4212–4217
34. Link S, El – Sayed MA (1999) Spectral properties and relaxation dynamics of surface plasmon electronic oscillations in gold and silver nanodots and nanorods. J Phy Chem B 103:8410–8426
35. Hyun BR, Zhong YW, Bartnik AC, Sun L, Abrun HD, Wise FW, Goodreau JD, Matthews JM, Leslie TM, Borrelli NF (2008) Plasmon - enhanced photocurrent using gold nanoparticles on a three-dimensional TiO_2 nanowire - web electrode. Acs Nano 2: 2206–2212
36. Ansari SA, Khan MM, Ansari MO, Cho MH (2015) Gold nanoparticles-sensitized wide and narrow band gap TiO_2 for visible light applications: A comparative study. New J Chem 39:4708–4815
37. Zolanvari A, Sadeghi H, Norouzi R, Ranjgar A (2013) Surface plasmons and optical properties of TiO_2/X (X=Au and Ag) nanostructure thin films. Chin Phy Lett 30:096201
38. Gonfa BA, Kim MR, Zheng P, Cushing S, Qiao Q, Nianqiang W, Khakania MAE, Ma D (2016) Investigation of plasmonic effect in air-processed PbS/CdS core-shell quantum dot based solar cells. J Mater Chem A 4:13071–13080
39. Barbero G (2017) Theoretical interpretation of Warburg's impedance in unsupported electrolytic cells. J Phy Chem Chem Phy 19: 32575–32579
40. Tian J, Lv L, Fei C, Wang Y, Liu X, Cao G (2014) A highly efficient (>6%) Cd1-xMnxSe quantum dot sensitized solar cell. J Mater Chem A 2:19653–19659
41. Kim HJ, Kim DJ, Rao SS, Savariraj AD, Soo-Kyoung K, Son MK, Gopi CVVM, Prabakar K (2014) Highly efficient solution processed nanorice structured NiS counter electrode for quantum dot sensitized solar cells. Electrochimica Acta 127:427–432
42. Punnoose D, Rao SS, Kim SK, Kim HJ (2015) Exploring the effect of manganese in lead sulfide quantum dot sensitized solar cell to enhance the photovoltaic performance. RSC Adv 5:33136–33145
43. Yen YC, Chen JA, Ou U, Chen YS, Lin KJ (2017) Plasmon - enhanced photocurrent using gold nanoparticles on a three-dimensional TiO_2 nanowire - web electrode. Sci Rep 7:42524